
Article:
Taras, P., Li, G.J. orcid.org/0000-0002-5956-4033 and Zhu, Z.Q. (2017) Comparative Study of Fault Tolerant Switched Flux Permanent Magnet Machines. IEEE Transactions on Industrial Electronics, 64 (3). pp. 1939-1948. ISSN 0278-0046

https://doi.org/10.1109/TIE.2016.2627022

Comparative Study of Fault Tolerant Switched Flux Permanent Magnet Machines

P. Taras, G. J. Li, Member, IEEE, and Z. Q. Zhu, Fellow, IEEE

Abstract— The fault tolerant capabilities are compared in this paper for the conventional double layer switched flux permanent magnet machine and its single layer counterparts, i.e. C-core, E-core and modular. The comparison includes the inter-turn short-circuit and irreversible demagnetization faults. A combination of Simulink and finite element models is used in the study. Based on the predictions, it is found that the modular topology produces the lowest short-circuit current and also has the best demagnetization withstand capability while the conventional one produces the highest short-circuit current and has the worst demagnetization withstand capability. The frozen permeability method is employed to separate the flux produced by armature current and magnets, and the results showed that, besides the influence of short-circuit current, the available magnet volume and magnetic circuit configuration play an important role in the demagnetization process. It is also found that removing half of the magnets, such as using C-core, E-core and modular topologies, generally improves the demagnetization withstand capability and also increases the torque per magnet volume. Measured results are also presented to validate the short-circuit current predictions and magnet demagnetization.

Index Terms— demagnetization, fault tolerance, fault tolerant control, permanent magnets, permanent magnet motors, reliability, short-circuit currents, temperature dependence.

NOMENCLATURE

B_r	Remanent flux density
e_a, e_b, e_c	Back-EMFs in phases a, b and c
f	Friction coefficient
$[\Phi_0]$	Open-circuit flux linkage vector
H	Magnetic field strength
H_k	Knee point magnetic field value
ib, ic	Currents in phases B and C
i_h, i_f	Currents in healthy and faulty components of phase A
J	Rotor moment of inertia
L_h, L_f	Self-inductances of healthy and faulty components of phase A
L_b, L_c	Self-inductances of phases B and C
M_{xy}	Mutual inductance between x and y where x and y can be any of the following: h, f, b, c
p	Number of pole pairs
R	Stator phase resistance
Ω	Mechanical speed
τ	Ratio of short-circuited turns to total number of turns per phase
θ_e	Electrical rotor position
T_{em}, T_{cogg}, T_{reluct}, T_{load}	Electromagnetic, cogging, reluctance and load torques
v_h, v_f	Voltages on healthy and faulty components of phase A
v_b,v_c	Voltages on phases B and C

I. INTRODUCTION

THE switched flux permanent magnet machine (SFPMM) has attracted much attention in recent years due to its high torque density and robust rotor structure which make it suitable for safety-critical and harsh environment applications such as aerospace and automotive [1], [2], [3], [4]. Compared with other rotor-mounted PM synchronous machines, the SFPMM exhibits some distinguished advantages [5], [6], [7]. The PMs and windings are both located on the stator, as shown in Fig. 1 (a), making them easier for cooling, whilst the rotor does not contain any PMs or windings and hence is much more robust and suitable for high speed applications. In addition, since the SFPMM employs non-overlapping, concentrated windings, the end-winding and consequently the copper loss is reduced, leading to potential increase in machine efficiency. Although SFPMM shares some of its advantages with other stator-mounted PM machines such as the doubly salient (DSPMM) and flux-reversal (FRPMM) permanent magnet machines, including the rotor simplicity and robustness, it exhibits bipolar flux linkage, making it possible to achieve higher torque density than the DSPMM in which the flux linkage is unipolar [8]. It also has a better PM placement compared to the FRPMM in which the magnets are subject to pulsating radial force and potential demagnetization [5].

The conventional SFPMM has a double layer winding configuration and hence it is not suitable for fault tolerant applications since there are no thermal, physical and magnetic separations between phases. This can be improved by adopting a single layer winding also known as the alternate poles wound SFPMM, in which only alternate stator poles are wound [9], [10], [11]. Several single layer SFPMM have been proposed in recent years. They are all based on the modification of the unwound stator teeth, e.g. the C-core topology [9], as shown in Fig. 1 (b), completely removes the unwound teeth, whilst the E-core topology, as shown in Fig. 1 (c), replaces the PMs from the unwound teeth with the same iron material as the stator iron core. If PMs in alternate stator teeth are removed, the modular topology can then be obtained, as shown in Fig. 1 (d) [10], which allows to achieve better fault-tolerant capability since the self-inductance increases whilst the mutual inductance decreases. In addition, the stator structure is simplified by using C-core, E-core and modular structures and the PM volume is reduced, which also leads to potential increase in the torque per PM volume.

However, an important issue of all the SFPMMs is the PM location, which is inside the concentrated armature coils, making them potentially vulnerable to demagnetization due to high temperatures and demagnetizing fields during flux weakening or short-circuit operation [12], [13], [14]. This would be a problem for instance in the aircraft applications where the machines often need to operate at high temperatures at around 150^{o}C, which can irreversibly demagnetize the PMs. Although important, the issue of demagnetization in the SFPMMs has been brought under investigation only recently. The available literature shows that the machine can withstand

demagnetization under generating and motoring operations, given that the PM temperature is kept low [15], [16], [17], [18]. The armature MMF is found to be always parallel to the PM MMF and hence will not demagnetize the magnets. In [16], an analysis of a SFPMM using ferrite as PM shows that local demagnetization occurs in the corners of the PM adjacent to the airgap leading to deteriorated machine performance. This occurs in both generating and motoring modes. In [17] a study considering PM dependence with temperature is carried out, showing the possibility of irreversible demagnetization at high temperatures. Finally, in [18] the demagnetization is assessed for a SFPMM having hybrid ferrite and NdFeB PMs at different temperatures.

TABLE I PARAMETERS OF THE INVESTIGATED MACHINES

Stator slot number	12	Stator yoke height (mm)	3.6
Rotor pole number	10	Stack length (mm)	25
Rated speed (rpm)	400	Air-gap length (mm)	0.5
Rated rms current (A)	11	Rotor outer radius (mm)	27.5
Rated torque (Nm)	2.2/1.5/2.0/1.8 *	Magnet thickness (mm)	3.6
Stator outer radius (mm)	45	Magnet remanence NdFeB (T)	1.2
Stator inner radius (mm)	28	Number of turns/phase	72

*Conventional/C-core/E-core/modular

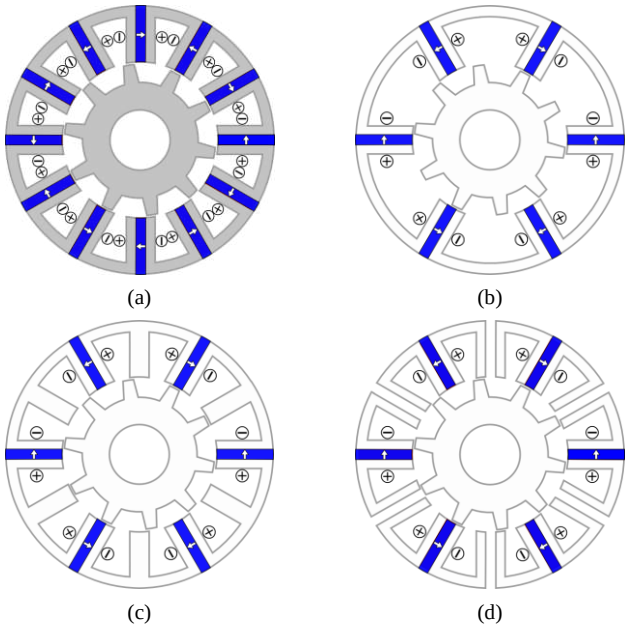

Fig. 1 Cross-sections of considered SFPMMs. (a) Conventional, (b) C-core, (c) E-core, (d) Modular.

However, in the available literature, only healthy conditions are considered and only the conventional topology is investigated. Moreover, the fault-tolerant topologies such as C-core, E-core and modular machines have been compared only from the point of view of electromagnetic performance and static characteristics but have not been studied under faulty operations, particularly under the inter-turn short-circuit conditions. Due to the specific topology of the SFPMM (PMs are surrounded by armature coils), the inter-turn short-circuit could have a dramatic effect on the affected PM. Therefore, to fill in this gap, in this paper the potential irreversible PM demagnetization due to inter-turn short-circuit of four SFPMM machines, i.e. conventional double layer, single layer C-core, E-core and modular machines, is investigated. Since the short-circuit fault can quickly lead to significant temperature increase, the temperature dependent properties of PM material are also considered in the study.

II. FEATURES OF INVESTIGATED MACHINES

The cross sections of the conventional and modular machines are shown in Fig. 1 while their main parameters are given in Table I. Compared with the conventional one, the C-core, E-core and modular topologies have the PM volume reduced by half and some of the PM magnetization directions changed in order to maintain an alternating polarity across the stator circumference. Giving the different magnet magnetization directions for the C-core, E-core and modular structures, the coil connections must also be changed, Fig. 1 (b) - Fig. 1 (d). Moreover, in case of the E-core and modular machines, the unwound stator teeth are modified by either removing the magnets or replacing the magnets with iron while the wound teeth containing the PM have the same geometries as those in the conventional machines. All machines have 3-phase winding, and all studied fault tolerant machines (C-core, E-core and modular) have two coils per phase while the conventional one has four coils per phase. However, to maintain similar phase back-EMF level, the number of turns per phase is the same for all investigated machines. The PM material used in all machines is NdFeB (N35 grade) [19].

As shown in [20], a link can be established between topologies from Fig. 1 (b) - Fig. 1 (d) based on a geometrical parameter named “flux gap” which quantifies the variation of the unwounded stator tooth width. Considering the modular topology, Fig. 1 (d), in which the PMs in alternate stator teeth are removed, leading to a flux gap opening of 7.5 mech. deg. The flux gap opening can be increased or reduced, leading to enlargement or reduction of the flux gap, as shown in Fig. 2. During this process, other machine dimensions are maintained constant. However, at some stage during the reduction process, Fig. 2 (c), the tooth sides adjacent to flux gaps will eventually overlap, leading to the dissapearance of the flux gap. At this point, the SFPMM becomes an E-core machine with a zero flux gap opening. Continuing the reduction of the flux gap opening will result in the reduction of the unwound stator tooth thickness until the lower negative limit of flux gaps (-15 degrees), for which the tooth dissappears, transforming the E-core topology to a C-core one, as shown in Fig. 2 (f). Therefore, the flux gap width ranges from -15 mech. deg. to 20.6 mech. deg., with the lower limit being given by the unwound tooth disappearance while the higher limit is imposed by the feasibility of the windings. It is worth mentioning that at a 7.5 deg. flux gap opening, the copper area is the same for both the modular and the conventional single layer machines as shown in Fig. 1. In this manner, a link between the three studied SFPMM is defined with the help of the flux gap parameter and the structural changes which affect the unwound teeth, such as:

- Modular machines with flux gaps (actual) – the flux gap ranges from 0 to 20.6 mech. deg. and the resulting stator is segmented as shown in Fig. 2 (a) to (c).
- E-core machines with a variable cross-section of the unwound tooth – the flux gap (virtual) interval is (-15, 0] mech. deg. as shown in Fig. 2 (d) to (e).
- C-core machine as shown in Fig. 2 (f), obtained from the E-core machines at the flux gap (virtual) of -15 mech. deg.

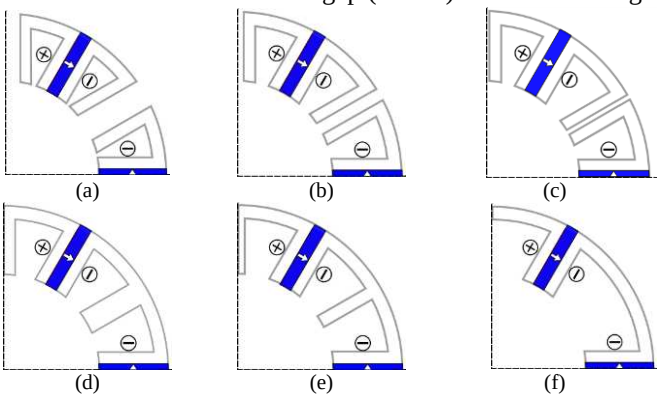

Fig. 2 Flux gap opening variation. (a) 20.6 deg., (b) 7.5 deg., (c) 3.75 deg, (d) 0 deg., (e) -7.5 deg., (f) -15 deg..

In this way, the C-core, E-core and modular machines can be studied and compared in a unified way by varying the flux gap opening, as shown in Fig. 3 and TABLE II. According to Fig. 3, the E-core topology produces the highest average torque. Although the E-core machine produces 10% lower average torque than its double layer conventional counterpart (TABLE II), it is still acceptable, given the fact that the PM volume is halved in the former. This also means that the E-core SFPMM makes better use of the available PMs. It is interesting to note that with the increasing flux gap opening, the performance of the E-core topology improves while for the modular topology the performance deteriorates. It can be concluded that the auxiliary unwounded tooth, without flux-gaps, is important in retaining as much performance as possible when compared with the conventional double layer SFPMM.

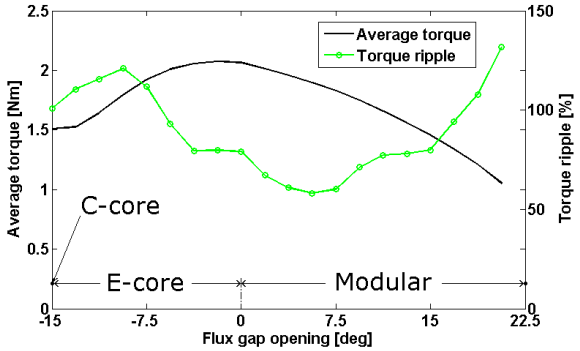

Fig. 3 Average torque and torque ripple variations against flux gap opening. Torque ripple is the peak-peak torque over average torque.

TABLE II PERFORMANCE COMPARISON

	Average torque [Nm]	Torque ripple [%]
Conventional	2.2	14
C-core	1.5	101
E-core	2.0	79
Modular (7.5 deg.)	1.8	60

In addition, the separation between phases and hence the fault tolerant capability can also be linked with the flux-gap parameter, e.g. higher flux-gap opening means stronger separation between phases. It is worth mentioning that the C-core topology (a highly un-optimized double layer machine from the point of view of slot/pole number combination) has similar features as the double layer conventional SFPMM, i.e. both have a strong mutual coupling between phases. This can be proven by the results shown in TABLE III in which the C-core topology has a comparable mutual inductance between phases with the conventional one (0.09 mH vs 0.12 mH). However, the modular machines with large flux gap openings have the lowest mutual inductance and hence provide the best magnetic, thermal and electrical decoupling between phases. The influence of flux gaps on mutual coupling between phases will have a profound influence on short-circuit current and the resulted magnet irreversible demagnetization as will be investigated in the following sections.

TABLE III AVERAGE SELF- AND MUTUAL INDUCTANCES

	Self inductance [mH]	Mutual inductance [mH]
Conventional	0.24	-0.12
C-core	0.47	0.09
E-core	0.57	0.05
Modular(7.5 deg.)	0.53	0.04

III. FAULT MODELLING OF SFPMM

A. Investigated Faults

The PM irreversible demagnetization fault under inter-turn short-circuit conditions is investigated in this paper. The inter-turn short-circuit fault is a severe condition [21], [22] which affects the machine operation and can lead to the destruction of the entire winding. High inter-turn short-circuit currents will lead to local overheating which can propagate further to the PMs placed inside the affected coils of the SFPMMs due to their specific stator topologies. As a result, the irreversible demagnetization fault could occur, lowering the PM remanent flux density (B_r) and hence the overall machine performance. By way of example, the short-circuit is introduced in phase A, as shown in Fig. 4 (a). Furthermore, it is assumed that if only one coil per phase is short-circuited, then for conventional machine the fault severity is 25% while for C-core, E-core and modular machines, it is 50%. Subsequent studies concerning the demagnetization will be focused on the PM inside the affected coil.

The PM material defined in finite element model has to account for changes in B_r due to irreversible demagnetization especially at higher temperatures [23], [24]. The PM model will update the B_r locally inside each mesh element if the magnetic field strength H drops below the knee point value H_k, as shown in Fig. 4 (b). The update algorithm is the following:

(1) initially the PM working point is defined by the point w which has a remanence of B_r;

(2) assuming the new working point is d and $H_d < H_k$, B_r will be updated to B_r';

(3) if the demagnetizing MMF is reduced, the new working point is *w'* along a recoil line defined by B_r'.

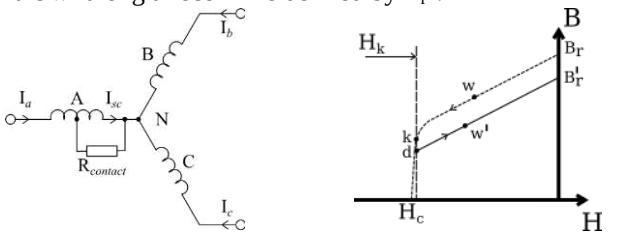

(a) (b)

Fig. 4 The faults investigated in this paper. (a) schematic representation of the inter-turn short-circuit fault, (b) the PM irreversible demagnetization model.

B. Method of Investigation

The investigation method adopted in this paper is based on a combination of FE (Cedrat/Flux2D) and MATLAB/Simulink models. Firstly, FE models are used to obtain the inductances, back-EMF and cogging torque waveforms which are temperature and rotor position dependent. These will be used later in phase variable models implemented in Simulink, which will then generate the armature currents under the inter-turn short-circuit conditions. Finally, these currents are introduced in the magneto-static FE models to assess the aforementioned demagnetization. It is worth noting that the solution of using FE and MATLAB/Simulink models is much faster than the co-simulation models while providing satisfactory accuracy.

C. Dynamic Model (Motoring Mode)

The dynamic operation model [11], [25], [26], [27], [28] that can be used for both healthy and faulty operations is based on Matlab/Simulink models and represented in Fig. 5. The SFPMM model can be implemented using equations (1) and (2) in the Appendix. The Maximum Torque per Ampere (MTPA) control strategy is used. The conditions imposed for all machines are the same rated current (11 Arms) and the same speed (1000 rpm) during healthy conditions. Initially, the machine operates under healthy conditions and then the inter-turn short-circuit is introduced in the phase A. The temperature rise effects are considered during the faulty operation for the short-circuited coil and the affected PM.

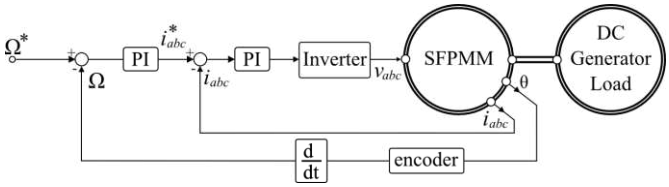

Fig. 5 The dynamic operation model.

Using this model, the short-circuit current can be calculated. The peak values during steady state regime for different temperatures are given in TABLE IV. It can be noticed that short-circuit current decreases with temperature. This is due to two reasons. First, the resistance of the affected coil increases with temperature. Second, remanence of the affected magnet and its contribution to the phase back-EMF decrease with temperature. Moreover, it is also found that the C-core, E-core and modular machines are characterized by a smaller short-circuit current as expected due to their higher self-inductance.

It should be noted that although the short-circuit current is much smaller for C-core, E-core and modular machines, the resulting demagnetizing MMF produced by the short-circuited coil will still be close to that of the conventional machine. This is due to the fact that the short-circuited coil contains a double number of turns for C-core, E-core and modular machines when compared with the conventional counterpart.

TABLE IV STEADY-STATE PEAK VALUES OF SHORT-CIRCUIT CURRENT 2000 RPM

Machines	25°C	50°C	75°C	100°C	125°C	150°C
Conventional	36.4	35.9	35.2	32.7	30.4	24.4
C-core	20.0	19.9	19.6	17.8	15.9	11.7
E-core	18.9	18.9	18.8	18.5	18.0	15.9
Modular	15.2	15.0	14.8	14.3	13.6	11.1

D. Experimental Validation of Faulty Model

Two prototypes (conventional and E-core machines) are used during experimental validation. Both machines have the 12-slot and 10-pole configurations as shown in Fig. 6. The dimensions of the conventional machine are given in TABLE I, while the E-core machine has the same parameters as in [29] and therefore not reproduced here. It should be mentioned that although the stator diameter and copper losses are the same, the split ratio is different between the two prototypes. However, the E-core prototype has the same rated current, the same number of turns per phase, the same slot area as the conventional one and hence the resulting short-circuit currents can be compared between the two machines.

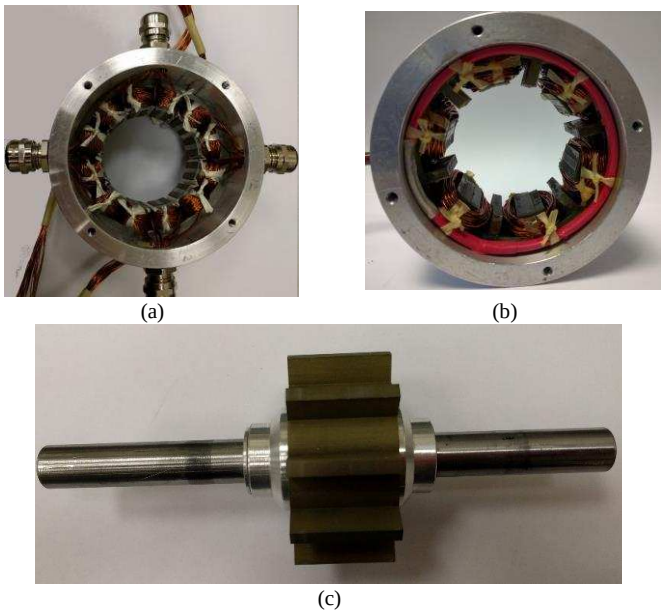

(a) (b)

(c)

Fig. 6 Prototypes of conventional and E-core SFPMMs with 12-slot/10-pole. (a) conventional stator, (b) E-core stator, (c) conventional rotor.

Dynamic tests have been carried out in motoring mode for both machines under the MTPA control strategy mentioned previously. The dynamic model discussed in the previous section is implemented using a dSPACE platform [11], an inverter and a DC machine as mechanical load. The speed and

torque are maintained at the same values during both healthy and faulty modes. By way of example, in case of the conventional machine, the phase A is affected and has one coil short-circuited (out of a total of 4) corresponding to a fault severity of 25%. For the E-core machine the 50% case is considered which also corresponds to one coil affected (out of 2 per phase). In both cases, the steady state peak to peak short-circuit current variation with speed is shown in Fig. 7. A good match can be observed between the predicted and measured results with errors less than 5%.

The predicted and measured currents in the affected coils, as well as speed waveforms before and after the inter-turn short-circuit, are shown in Fig. 8 for a speed of 1000 rpm.

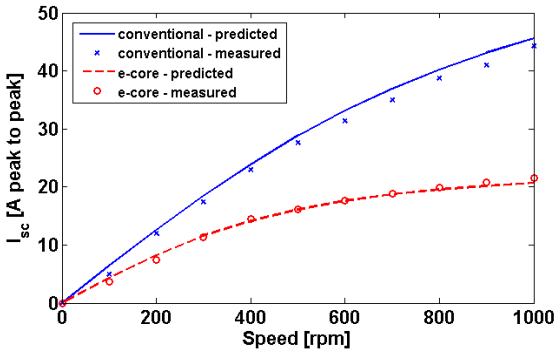

Fig. 7 Steady state peak to peak short-circuit current vs rotor speed for conventional/one coil and E-core/one coil short-circuit operation in motoring mode.

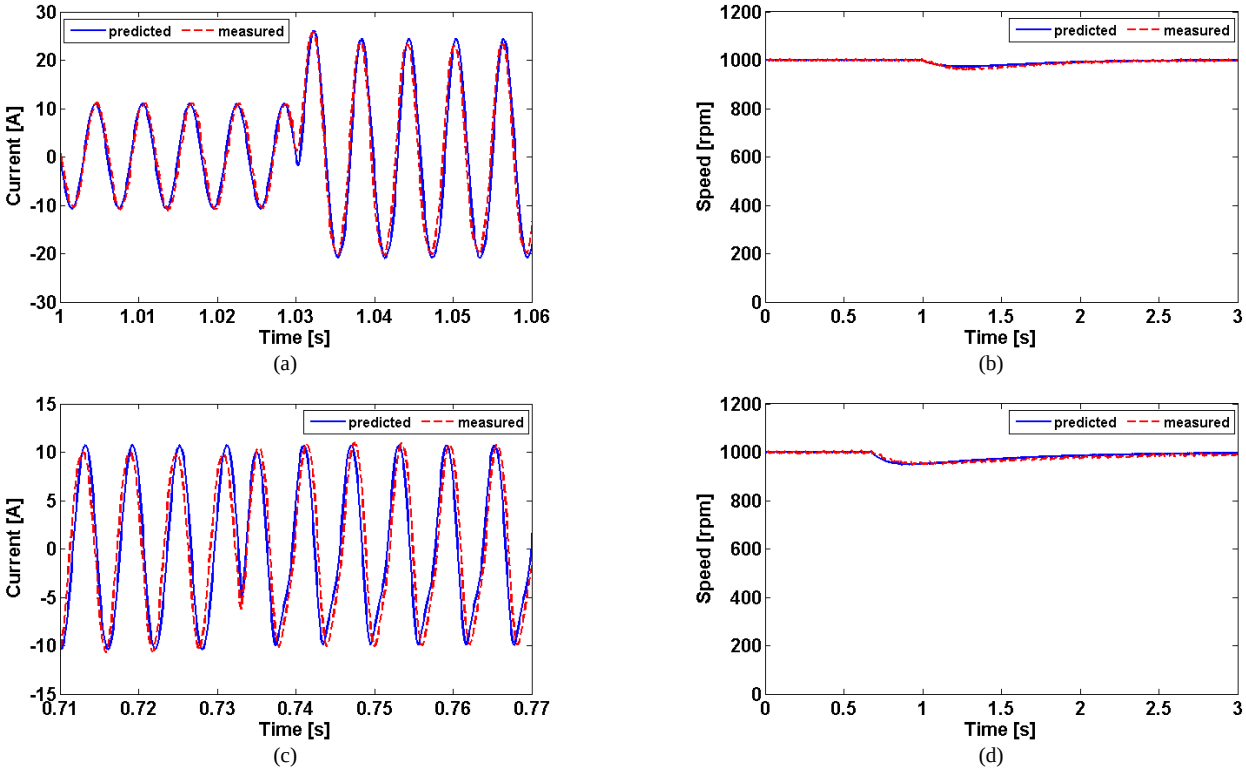

Fig. 8 Predicted and measured currents in the affected coil and speeds. (a) conventional - current, (b) conventional - speed, (c) E-core – current, (d) E-core - speed.

IV. Comparison of SFPMMs Demagnetization Withstand Capability

As a direct consequence of the short-circuit current, a demagnetizing MMF is developed, which could cause irreversible magnet demagnetization. Therefore, a comparison is carried out in terms of demagnetization withstand capability for the conventional, C-core, E-core and modular SFPMMs under the aforementioned short-circuit conditions. Two cases are considered – the first one concerns local over-heating of the affected PM and short-circuited coil while other coils and magnets working at normal operating temperature. The second one assumes fault operation under short-circuit while all the magnets and coils are working at the same temperature, e.g. 100°C – global over-heating. For both cases, only one coil of phase A is short-circuited.

A. Local Over-Heating Case

The color maps of the flux density component parallel with the magnetization direction in the affected PM are shown in Fig. 9 for low and high temperature cases. The color map scale is upper limited by the knee point value of the affected magnet to show only the irreversibly demagnetized areas. The negative q-axis rotor position (rotor tooth is aligned with the affected PM) is chosen as being representative, since the PM working point is the lowest in this position. Only the conventional and E-core cases are represented as the C-core and modular topologies yield results similar to the E-core one. It can be seen at low temperature (25°C) that the demagnetization effect is local and confined at the bottom corners of the PMs. This

effect was noticed during healthy conditions as well for SFPMM using ferrite magnets [16]. However, at high temperature (100°C), total PM demagnetization occurs for the conventional machine as shown in Fig. 9 (c), while for the E-core the demagnetization is limited to only half of the PM, Fig. 9 (d). This is due to PM material high knee point (0.28 T for 100°C). For 150°C, the knee point value is even higher (0.5 T), and irreversible demagnetization occurs throughout the entire affected PM for all studied topologies.

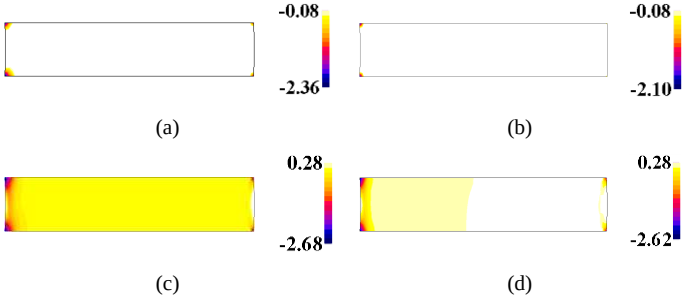

Fig. 9 Demagnetization flux density colour maps (white – not demagnetized, coloured – demagnetized) with short-circuit fault at 1000 rpm. (a) conventional 25° C, (b) E-core 25° C, (c) conventional 100° C, (d) E-core 100° C.

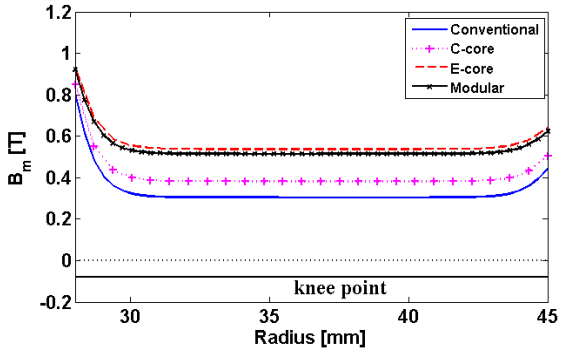

Fig. 10 Flux densities (circumferential components) along the central line of the affected PM. (a) 25°C, (b) 100°C.

The flux density colour maps in Fig. 9 only show the irreversibly demagnetized areas, but they cannot easily quantify the severity of the demagnetization. In order to do so, the flux density (circumferential component) along the central line of the affected PM is used. The results for low temperature (25°C) are shown in Fig. 10 (a). The knee point value is also given so that the plots can be compared against it in order to indicate if the irreversible demagnetization has occurred or not. Although none of the topologies is irreversibly demagnetized at this low temperature, the conventional and C-core topologies have lower magnet working points when compared with others, leading to narrower margin to the irreversible demagnetization.

The results for 100°C are shown in Fig. 10 (b). Similar to the previous results, the PM working points of the E-core and modular machines are higher than the conventional and C-core counterparts. Most importantly, for the modular machine, most part of the affected PM is not irreversibly demagnetized except for the edge effect at the bottom of the PM. The results for 150°C have also been obtained, which have similar trend as for 100°C, but the affected PM for all topologies has been irreversibly demagnetized although the demagnetization levels for E-core and modular machines are lower than the C-core and conventional machines. It is also found that the modular machine can withstand at least a temperature of 25°C higher than the conventional and C-core machines as shown in TABLE V which summarizes the demagnetization occurrence over a wide range of operating temperatures from 25°C to 150°C for the studied topologies:

TABLE V IRREVERSIBLE DEMAGNETIZATION VS. TEMPERATURE

	conventional	C-core	E-core	modular
25 °C	no	no	no	no
50 °C	no	no	no	no
75 °C	no	no	no	no
100 °C	yes	yes	yes	no
125 °C	yes	yes	yes	yes
150 °C	yes	yes	yes	yes

*yes means irreversible demagnetization has occurred in more than 50% of the area of affected PM.

In order to explain why different machine topologies have different irreversible demagnetization withstand capabilities, the frozen permeability (FP) method is employed. Using the FP method, the affected PM can be artificially removed from the FE model without affecting the working point of PMs and the saturation level of stator and rotor iron cores. In such a way, the influence of mutual coupling between adjacent phases and PMs on the affected magnet can be accurately investigated. Fig. 11 shows the flux produced by healthy PMs along with all the current sources (healthy and short-circuited). The conclusion is that the rest of the magnetic circuit has a demagnetizing effect over the affected PM since the flux lines are crossing through the affected PM on the opposite direction to its magnetization.

Looking at the local flux patterns circled by the dashed, fan-shaped curve from Fig. 11, it can be seen that the conventional and C-core topologies are quite similar. The demagnetizing flux produced by the rest of the magnetic circuit is flowing freely through the affected PM. This explains in turn why they both present the worst demagnetization withstand capability. The E-core machine, however, diverts some of the demagnetizing flux through its magnetless tooth, leading to improved demagnetization withstand capability. The modular topology appears to be the best solution amongst all the investigated topologies, with the demagnetizing flux being both diverted but also reduced due to the presence of unwound

teeth with flux gaps (increased reluctance). It is worth noting that the previous analysis was carried out at low temperature and short-circuit conditions. However, the results can be extended to higher temperatures under both healthy and short-circuit conditions.

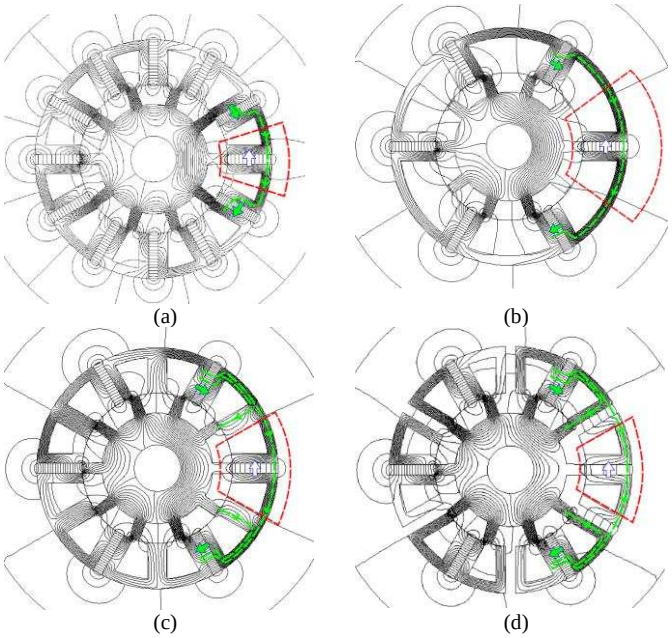

Fig. 11 Flux lines produced by PMs & armature currents after removing the affected magnet at 25°C. (a) Conventional, (b) C-core, (c) E-core, (d) Modular.

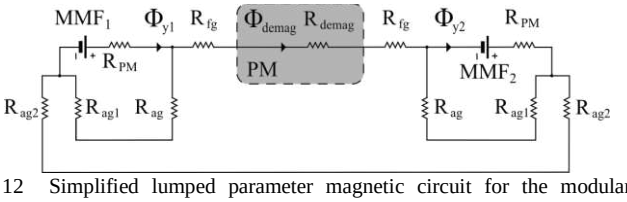

Fig. 12 Simplified lumped parameter magnetic circuit for the modular topologies.

A lumped parameter magnetic circuit can also be employed, Fig. 12, to explain the previous results. By way of example, only the modular topology is detailed. However, the circuit in Fig. 12 can be adopted for the rest of studied machines with appropriate modification. The adjacent PMs are represented by the MMF_1 and MMF_2 which produce flux Φ_{y1} and Φ_{y2}. Φ_{demag} represents the demagnetizing flux through the affected PM. R_{demag} and R_{PM} are reluctances characterizing the affected and adjacent PMs. R_{ag}, R_{ag1} and R_{ag2} are reluctances determined by airgap and different overlapping sections between the stator and rotor teeth. R_{ag} in particular is the airgap reluctance defined between the magnetless stator tooth and the rotor tooth. The flux-gap reluctance is represented by R_{fg}. For modular and E-core topologies part of potentially demagnetizing fluxes Φ_{y1} and Φ_{y2} can be diverted through R_{ag} circuit branch and also reduced by the extra R_{fg} thus minimizing the Φ_{demag} component. Therefore, a modular topology will limit the demagnetizing influence of the rest of the magnetic circuit by either diverting the flux from the concerned area (through R_{ag}) or reducing it (though flux-gap).

B. Global Over-Heating Case

In this section it is assumed that the entire machine is exposed to the same high temperature while working under one coil short-circuited condition. By way of example, 100°C is chosen as the working temperature for all PMs and windings. As investigated in previous sections, it is the threshold temperature beyond which the modular machine starts to be irreversibly demagnetized.

The short-circuit currents obtained for the new case are compared with previous results (only one PM is working at 100°C), as shown in TABLE VI. In this case, it is found that the short-circuit currents are all higher than the local over-heating case.

TABLE VI SHORT-CIRCUIT CURRENT COMPARISON

	conventional	C-core	E-core	modular
one PM	32.7	17.7	18.5	14.3
all PMs	35.2	20.6	18.8	14.6

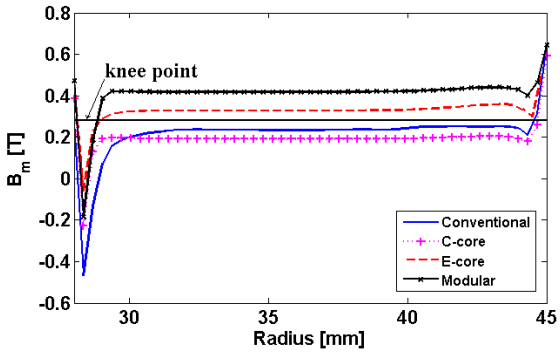

Fig. 13 Flux densities (circumferential components) along the central line of the affected PM (all PMs at 100°C).

From Fig. 13 it can be noticed that the working point of the PMs is generally higher for all PMs at 100°C case than the previous case where only the affected magnet is working at 100°C. Moreover, the E-core and modular topologies can both safely withstand demagnetization although the edge adjacent to the airgap is still irreversibly demagnetized. This is mainly due to the fact that the adjacent PMs are much weaker in this case, generating smaller demagnetizing MMF.

C. Experimental Validation of Temperature Effect on PMs

In this section, experimental results concerning the variation of PM working point with temperature (and hence indirect validation of reversible demagnetization) are presented for the conventional double layer prototype. This is done by using four type-K thermocouples mounted on two adjacent PMs and the corresponding coils, as shown in Fig. 14. The thermocouples for measuring winding temperatures are buried deep in the stator slots while the PM ones are located at the lateral end of the PMs.

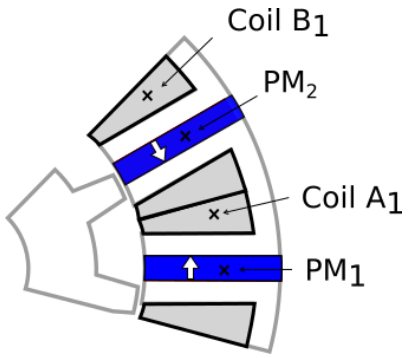

Fig. 14 Locations of thermocouples.

TABLE VII FINAL LOCAL TEMPERATURES

	PM_1	Coil A_1	Coil B_1	PM_2
Temperature [°C]	63	106	66	51

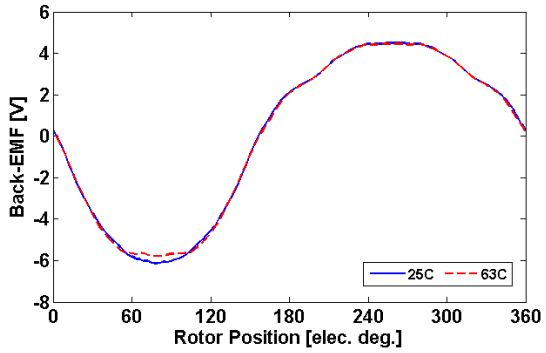

(a)

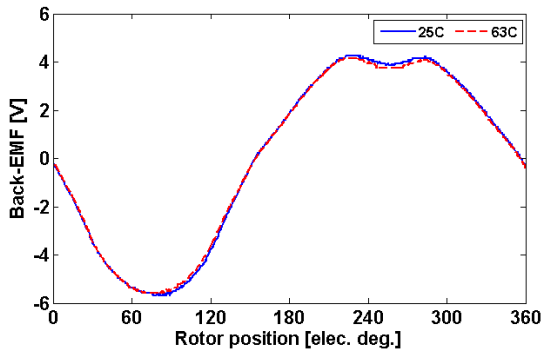

(b)

Fig. 15 Coil A_1 back-EMF. Waveforms for 25°C and 63°C. (a) predicted, (b) measured.

The purpose of the experiment is to show the back-EMF variation due to temperature increase in the affected PM. The experiment is conducted in open-circuit generator mode since it is found that the magnet demagnetization is mainly due to adjacent magnets rather than armature currents (healthy and short-circuit). The methodology is as follows. First, back-EMF of the coil A1 is measured at low temperature (25°C). Next, the coil A1 is short-circuited, while the rotor speed is very high (2000 rpm) in order to produce a high-short-circuit current that will increase the temperature of PM_1 (63°C), as shown in TABLE VII. The PM_1 temperature of 63°C corresponds to 106°C in the coil A_1. After the desirable temperature has been reached on the affected PM (PM_1), the short-circuit is removed and the back-EMF of the coil A_1 is measured again. A drop of 3% in the back-EMF confirms the expected outcome that the magnet is reversibly demagnetized due to the temperature rise, as shown in Fig. 15. The threshold PM temperature (100°C) for irreversible demagnetization has not been reached in order to protect the machine because it will be used for future investigations.

V. CONCLUSIONS

Three modular single layer SFPMMs are investigated and compared with their conventional double layer counterparts in terms of machine performance, short-circuit current and demagnetization withstand capability. This research is original and has not been carried out in previous works. TABLE VIII summarizes the main features of each topology.

TABLE VIII SUMMARY OF THE STUDIED TOPOLOGIES

	Conventional	C-core	E-core	Modular
Av. Torque [Nm]	2.2	1.5	2.0	1.8
Torque/PM vol. [Nm/m^3]	1.44e6	1.96e6	2.61e6	2.35e6
I_{sc} at 25°C [A]	36.4	20	18.9	15.2
DWC	poor	poor	good	best

* DWC: demagnetization withstanding capability

It is found that the reduction of the PM volume affects both performance and demagnetization withstand capabilities. There is a performance penalty in adopting fault tolerant solutions such as E-core and modular topologies (for instance a drop in the torque capability and lower power factor due to increased phase self-inductance). However, their demagnetization withstand capability improves compared with conventional and C-core machines. This is mainly due to the fact that the magnetless stator teeth of the E-core and modular machines divert some of the demagnetizing flux produced by the remaining healthy parts of the magnetic circuit, protecting the affected PM against the irreversible demagnetization. As a result, better phase magnetic separation and also better demagnetization withstand capability can be achieved. It can be concluded that a good compromise between performance (average torque and torque ripple) and fault-tolerant capability would be using a modular topology with a small flux gaps which leads to an average torque drop slightly higher than 10% while being able to withstand a temperature of around 25°C higher than its conventional counterparts. The modular machine can be developed further so the flux gaps can be used for cooling, allowing the machine to work at higher phase currents and to improve the torque/mass ratio. Therefore, the thermal aspect will be developed further in future studies. The resulting high performance, fault tolerant capability and reduced price will make the modular topology well suitable for aerospace and electric and hybrid electric vehicles applications.

APPENDIX

The electrical model implemented in Matlab/Simulink is given by:

$$[v]=[R]\cdot[i]+\frac{d([L]\cdot[i])}{dt}+[e_0] \quad (1)$$

where [v], [i] and [e_0] are the phase voltage, phase current and back-EMF vectors. The [R] and [L] quantities are the matrices of the phase resistance and self- and mutual- inductances. The mechanical model is described by:

$$T_{em} + T_{cogg} + T_{reluct} = p \cdot [\Phi_0]^t \cdot [i] = J \cdot \frac{d\Omega}{dt} + f \cdot \Omega + T_{load} \quad (2)$$

where p = 10. For SFPMMs, the average reluctance torque is negligible under healthy conditions but can play a non-negligible role during short-circuit operations [30]. The dimension of the vectors involved in equations (1) and (2) is associated with the number of phases. Since the fault is also considered, an extra term is added to describe the short-circuited coil. The τ (%) is introduced to quantify the severity of the fault. The vectors from equations (1) can be rewritten such as:

$$[v] = \begin{bmatrix} v_h \\ v_b \\ v_c \\ v_f \end{bmatrix}, [i] = \begin{bmatrix} i_h \\ i_b \\ i_c \\ i_f \end{bmatrix}, [e_0] = \begin{bmatrix} (1-\tau) \cdot e_a \\ e_b \\ e_c \\ \tau \cdot e_a \end{bmatrix} \quad (3)$$

where h and f are indexes describing the faulty and healthy components of the affected phase. The flux vector can be expressed similarly as the back-EMF vector. The [R] and [L] are given by:

$$[R] = \begin{bmatrix} (1-\tau) \cdot R & 0 & 0 & 0 \\ 0 & R & 0 & 0 \\ 0 & 0 & R & 0 \\ 0 & 0 & 0 & \tau \cdot R \end{bmatrix},$$
$$[L(\theta_e)] = \begin{bmatrix} L_h & M_{Bh} & M_{Ch} & M_{fh} \\ M_{hB} & L_B & M_{CB} & M_{fB} \\ M_{hC} & M_{BC} & L_C & M_{fC} \\ M_{hf} & M_{Bf} & M_{Cf} & L_f \end{bmatrix} \quad (4)$$

The main diagonal of [L] represent self-inductances characterizing each phase, as well as the faulty part, while the rest of the terms represent mutual inductances, which are all calculated using finite element method.

REFERENCES

[1] G. Zhang, W. Hua, M. Cheng and J. Liao, "Design and comparison of two six-phase hybrid-excited flux-switching machines for EV/HEV applications," IEEE Trans. Ind. Electron., vol. 63, no. 1, pp. 481-493, Jan. 2016.

[2] T. Raminosoa, G. Gerada and M. Galea, "Design considerations for a fault-tolerant flux-switching permanent-magnet machine," IEEE Trans. Ind. Electron., vol. 58, no. 7, pp. 2818-2825, July 2011.

[3] Y. Shi, L. Jian, J. Wei, Z. Shao, W. Li and C. C. Chan, "A new perspective on the operating principle of flux-switching permanent-magnet machines," IEEE Trans. Ind. Electron., vol. 63, no. 3, pp. 1425-1437, March 2016.

[4] P. E. Kakosimos, A. G. Sarigiannidis, M. E. Beniakar, A. G. Kladas and C. Gerada, "Induction motors versus permanent-magnet actuators for aerospace applications," IEEE Trans. Ind. Electron., vol. 61, no. 8, pp. 4315-4325, Aug. 2014.

[5] M. Cheng, W. Hua, J. Zhang and W. Zhao, "Overview of stator-permanent magnet brushless machines," IEEE Trans. Ind. Electron., vol. 58, no. 11, pp. 5087-5101, Nov. 2011.

[6] A. Fasolo, L. Alberti and N. Bianchi, "Performance comparison between switching-flux and IPM machine with rare earth and ferrite PMs," in Proc. ICEM, Marseille, France, 2-5 Sept. 2012.

[7] W. Hua, M. Cheng, Z. Q. Zhu and W. X. Zhao, "Comparison of electromagnetic performance of brushless machiness having magnets in stator and rotor," J. Appl. Phys., vol. 103, no. 7, March 2008.

[8] W. Hua, Z. Q. Zhu, M. Cheng and Y. Pang, "Comparison of flux-switching and doubly-salient permanent magnet brushless machines," in Proc. ICEMS, Nanjing, China, 27-29 Sept. 2005.

[9] Z. Q. Zhu and J. T. Chen, "Advanced flux-switching permanent magnet brushless machines," IEEE Trans. Magn., vol. 46, no. 6, pp. 1447-1453, June 2010.

[10] R. L. Owen, Z. Q. Zhu, A. S. Thomas, G. W. Jewell and D. Howe, "Alternate poles wound flux-switching PM brushless AC machines," IEEE Trans. Ind. Appl., vol. 46, no. 2, pp. 790-797, March-April 2010.

[11] G. J. Li, J. Ojeda, E. Hoang and M. Gabsi, "Double and single layers flux-switching permanent magnet motors: Fault tolerant model for critical applications," in ICEMS, Beijing, 20-23 Aug. 2011.

[12] G. Zhao, L. Tian, Q. Shen and R. Tang, "Demagnetization analysis of permanent magnet synchronous machines under short circuit fault," in Proc. of APPEEC 2010, Chengdu, 28-31 March 2010.

[13] S. Ruoho, J. Kolehmainen, J. Ikäheimo and A. Arkkio, "Interdependence of demagnetization, loading, and temperature rise in a permanent-magnet synchronous motor," IEEE Trans. Magn., vol. 46, no. 3, pp. 949-953, March 2010.

[14] P. Zhou, D. Lin, Y. Xiao, N. Lambert and M. A. Rahman, "Temperature-dependent demagnetization model of permanent magnets for finite element analysis," IEEE Trans. Magn., vol. 48, no. 2, pp. 1031-1034, Feb. 2012.

[15] J. D. McFarland, T. M. Jahns and A. M. EL-Refaie, "Demagnetization performance characteristics of flux switching permanent magnet machines," in Proc. ICEM2014, Berlin, Germany, 2-5 Sept. 2014.

[16] S. Li, Y. Li and B. Sarlioglu, "Partial irreversible demagnetization assessment of flux switching permanent magnet machine using ferrite permanent magnet material," IEEE Trans. Magn., vol. 51, no. 7, pp. 1-9, July 2015.

[17] S. Zhu, M. Cheng, W. Hua and X. Cai, "Finite element analysis of flux-switching PM machine considering oversaturation and irreversible demagnetization," IEEE Trans. Magn., vol. 51, no. 11, pp. 1-4, Nov. 2015.

[18] I. A. A. Afinowi, Z. Q. Zhu, Y. Guan, J. C. Mipo and P. Farah, "Performance analysis of switched-flux machines with hybrid NdFeB and ferrite magnets," in Proc. of ICEMS 2014, Hangzhou, 22-25 Oct. 2014.

[19] "Arnold Magnetic Technologies," [Online]. Available: http://www.arnoldmagnetics.com/uploadedFiles/Library/pdf/Neo%20-%20Combined%20-%20140112.pdf. [Accessed 2015].

[20] P. Taras, G. J. Li and Z. Q. Zhu, "Comparative study of alternative modular switched flux permanent magnet machines," in Proc. ICIT, Seville, 17-19 March 2015.

[21] A. Bellini, F. Filippetti, C. Tassoni and G. A. Capolino, "Advances in diagnostic techniques for induction machines," IEEE Trans. Ind. Electron., vol. 55, no. 12, pp. 4109-4126, Dec. 2008.

[22] B. Sen, J. Wang and P. Lazari, "A high-fidelity computationally efficient transient model of interior permanent-magnet machine with stator turn fault," IEEE Trans. Ind. Electron., vol. 63, no. 2, pp. 773-783, Feb. 2016.

[23] S. Nair, V. I. Patel and J. Wang, "Post-demagnetization performance assessment for interior permanent magnet AC machines," IEEE Trans. Magn., vol. 52, no. 4, pp. 1-10, April 2016.

[24] K. T. Kim, Y. S. Lee and J. Hur, "Transient analysis of irreversible demagnetization of permenent magnet brushless DC motor with stator turn fault under the operating state," IEEE Trans. Ind. Appl., vol. 50, no. 5, pp. 3357-3364, Sept.-Oct. 2014.

[25] O. A. Mohammed, S. Liu and Z. Liu, "Physical modeling of PM synchronous motors for integrated coupling with machine drives," IEEE Trans. Magn., vol. 41, no. 5, pp. 1628 - 1631, May 2005.

[26] B. Vaseghi, B. Nahid-Mobarakh, N. Takorabet and F. Meibody-Tabar, "Inductance identification and study of PM motor with winding turn short circuit fault," IEEE Trans. Magn., vol. 47, no. 5, pp. 978-981, May 2011.

[27] L. Romeral, J. C. Urresty, J. R. Riba Ruiz and A. Garcia Espinosa,

"Modeling of surface-mounted permanent magnet synchronous motors with stator winding interturn faults," IEEE Trans. Ind. Electron., vol. 58, no. 5, pp. 1576-1585, May 2011.

[28] N. Leboeuf, T. Boileau, B. Nahid-Mobarakeh, N. Takorabet, F. Meibody-Tabar and G. Clerc, "Effects of imperfect manufacturing process on electromagnetic performance and online interturn fault detection in PMSMs," IEEE Trans. Ind. Electron., vol. 62, no. 6, pp. 3388-3398, June 2015.

[29] J. T. Chen, Z. Q. Zhu, S. Iwasaki and R. P. Deodhar, "A novel E-core switched-flux PM brushless AC machine," IEEE Trans Ind. Appl., vol. 47, no. 3, pp. 1273-1282, May-June 2011.

[30] E. Ben Sedrine, J. Ojeda, M. Gabsi and I. Slama-Belkhodja, "Fault-tolerant control using the GA optimization considering the reluctance torque of a five-phase flux switching machine," IEEE Trans. Energy Convers., vol. 30, no. 3, pp. 927-938, Sept. 2015.